HHS Public Access

Author manuscript

Am J Reprod Immunol. Author manuscript; available in PMC 2024 October 01.

Published in final edited form as:

Am J Reprod Immunol. 2023 October ; 90(4): e13773. doi:10.1111/aji.13773.

Western-Style Diet in the Presence of Elevated Circulating Testosterone Induces Adipocyte Hypertrophy without Proinflammatory Responses in Rhesus Macaques

Benjamin J. Burwitz[1,2,*], **Sofiya Yusova**[2], **Jacob J. Robino**[2], **Diana Takahashi**[2], **Addie Luo**[3], **Ov D. Slayden**[3], **Cecily V. Bishop**[3,4], **Jon D. Hennebold**[3], **Charles T. Roberts Jr.**[2,3], **Oleg Varlamov**[2,*]

[1]Divisions of Pathobiology and Immunology

[2]Divisions of Metabolic Health and Disease

[3]Reproductive and Developmental Sciences, Oregon National Primate Research Center

[4]Department of Animal and Rangeland Sciences, Oregon State University, Corvallis, OR 97331, USA.

Abstract

Anovulatory infertility is commonly associated with hyperandrogenemia (elevated testosterone, T), insulin resistance, obesity, and white adipose tissue (WAT) dysfunction associated with adipocyte hypertrophy. However, whether hyperandrogenemia and adipocyte hypertrophy per se induce a proinflammatory response is unknown. To address this question, we studied a group of young adult female nonhuman primates (NHP; rhesus macaques) exposed to a low-fat control diet and a group treated with an obesogenic Western-style diet (WSD) in the presence of elevated circulating testosterone (T+WSD). Immune cells residing in visceral omental white adipose tissue (OM-WAT), corpus luteum and the contralateral ovary, endometrium, lymph nodes, bone marrow, and peripheral blood mononuclear cells were characterized by flow cytometry during the luteal phase of the reproductive cycle. Following one year of treatment, T+WSD animals became more insulin-resistant and exhibited increased body fat and adipocyte hypertrophy compared to controls. T+WSD treatment did not induce macrophage polarization towards a proinflammatory phenotype in the tissues examined. Additionally, T+WSD treatment did not affect TNFα production by bone marrow macrophages in response to toll-like receptor agonists. While the major lymphoid subsets were not significantly affected by T+WSD treatment, we observed a significant reduction

[*]**Corresponding authors**: Ben Burwitz, PhD (burwitz@ohsu.edu), and Oleg Varlamov, MD, PhD (varlamov@ohsu.edu), Oregon National Primate Research Center, 505 NW 185[th] Ave, Beaverton OR 97006, USA.

Statement of contribution for authors

BJB designed the study and edited the manuscript; SY conducted flow cytometry experiments; JJR isolated cells; DT conducted animal experiments; AL isolated cells; ODS designed the study and edited the manuscript; CVB isolated cells; JDH designed the study and edited the manuscript; CR designed the study and edited the manuscript; OV designed the study, conducted experiments, and wrote the manuscript.

Conflict of interest Disclosure

The authors have nothing to disclose

Ethical statement

This study was approved by the Oregon National Primate Research Center Institutional Animal Care and Use Committee and conforms to current Office of Laboratory Animal Welfare regulations as stipulated in assurance number A3304–01.

in the frequency of effector memory CD8+ T-cells (Tem) in OM-WAT, but not in other tissues. Notably, OM-WAT Tem frequencies were negatively correlated with insulin resistance as assessed by Homeostatic Model Assessment for Insulin Resistance (HOMA-IR). Collectively, our data show that short-term T+WSD treatment induces weight gain, insulin resistance, and adipocyte hypertrophy, but does not have a significant effect on systemic and tissue-resident proinflammatory markers, suggesting that adipocyte hypertrophy and mild hyperandrogenemia alone are not sufficient to induce a proinflammatory response.

Keywords

Obesity; Western-style diet; PCOS; hyperandrogenemia; adipose tissue; insulin resistance; memory T-cells; macrophages; inflammation; nonhuman primates

Introduction

Reproductive tract dysfunction and subfertility or infertility are associated with hyperandrogenemia (elevated testosterone, T) and metabolic abnormalities, including insulin resistance, obesity, and white adipose tissue (WAT) dysfunction. Hyperandrogenemia and metabolic dysfunction are hallmarks of polycystic ovary syndrome (PCOS), which can have varying degrees of ovulatory dysfunction and the development of arrested antral follicles that give rise to “cystic” appearing ovaries [1–3]. Adipocyte hypertrophy, induced by obesity and hyperandrogenemia, has been suggested to contribute to the systemic low-grade inflammation [4–7] thought to be one of the drivers leading to reproductive dysfunction in women with PCOS [8].

Therefore, the primary objective of this study was to focus on the metabolic and immunological effects of an obesogenic high-fat Western-style diet (WSD) and mild hyperandrogenemia (T+WSD) on the systemic and tissue-resident proinflammatory milieu using a nonhuman primate (NHP) model. We have previously demonstrated that chronic consumption of a WSD in combination with mild hyperandrogenemia induced greater metabolic and WAT dysfunction in female rhesus macaques than in either treatment alone [9–11]. In these earlier studies, elevated T and WSD consumption were initiated at puberty, resulting in an increase in body fat mass and insulin resistance following three years of treatment [10,11]. To address the effects of T+WSD in the absence of simultaneous peripubertal developmental endocrine effects, we generated a cohort of six-year-old adult female rhesus macaques exposed to a low-fat diet and no exogenous T (controls) versus those treated with T+WSD for one year (Figure 1A). Individual treatments (i.e., T or WSD alone) were not included in this study because we previously determined that combined treatment led to earlier and more severe metabolic [10,11] and reproductive imparements, including increased numbers of arrested antral follicles and reduced fertility [12,13].

We determined the proinflammatory responses of tissue-resident immune cells by flow cytometry and assessed systemic inflammation by measuring the levels of circulating proinflammatory mediators (Figure 1A). To test whether T+WSD disrupts the immune milieu that may affect normal egg implantation and other relevant reproductive processes, we conducted immune cell profiling during the mid-luteal phase, the interval during the

menstrual cycle when the uterine endometrium is permissive for embryo implantation. Immune cells residing in omental (OM)-WAT, the corpus lutetium (CL), the contralateral ovary (OV) not containing the CL, endometrium (ENDO), lymph nodes (LNs), bone marrow (BM; a source of myeloid cells [14,15]), and peripheral blood mononuclear cells (PBMCs) were characterized by flow cytometry, using NHP-specific antibodies [16,17] (Figure 1A).

Our study demonstrates that T+WSD treatment of adult female rhesus macaques increases fat mass and induces insulin resistance and adipocyte hypertrophy, but has no significant effect on systemic or tissue-resident proinflammatory markers, suggesting that hyperandrogenemia and adipocyte hypertrophy alone are not sufficient to trigger a proinflammatory response.

Materials and Methods

Animal studies

This study was approved by the Oregon National Primate Research Center Institutional Animal Care and Use Committee and conforms to current Office of Laboratory Animal Welfare regulations as stipulated in assurance number A3304–01. Adult female rhesus macaques were pair-housed, with the cage size adjusted to animal weight according to the USDA Cage Size Guide, eighth Edition. Animals were maintained on either a monkey chow diet (n=5 Control; average age 6.04 ± 1.03) consisting of two daily meals of fiber-balanced monkey diet (15% calories from fat, 27% from protein and 59% from carbohydrates; no. 5052; Lab Diet, St. Louis, MO), supplemented with fruits and vegetables, or a WSD (n=9, average age 6.3 ± 0.57), containing 36% calories from fat, 18% from protein and 45% from carbohydrates (TAD Primate Diet 5LOP, 5A1F, Lab Diet), as previously described [10]. All WSD females also received testosterone implants as previously described [10]. Briefly, T-releasing capsules were prepared by packing Silastic tubing (0.34 cm i.d.; 0.64 cm o.d.; Dow Corning, Midland MI) with a mixture of cholesterol and T (Sigma-Aldrich, St. Louis, MO) at a ratio of 9:1. The capsules were implanted subcutaneously in the interscapular region. Weekly blood samples were assayed for serum T, and when levels dropped below 1.0 ng/ml, the capsules were replaced. A target range of ~1.5 ng/ml was maintained by changing the length of the T-releasing capsules from 1 to 5 cm over the study period. Androgen levels of T+WSD treated animals (Table 1) are in the range for women with hyperandrogenemia/PCOS [18–20]. Two experimental groups, designated Control (n=5) and T + WSD (Treated; n=9), were used in this study. Both animal groups were maintained for 12 months prior to necropsy. Two months before necropsy, all animals underwent a controlled ovarian stimulation protocol to collect oocytes for analyses of the meiotic maturation, fertilization rate, and embryo development (data not shown, separate manuscript in preparation). Animals were allowed to undergo one menstrual cycle before tissues were collected for this study.

Metabolic assays

Dual-energy X-ray absorptiometry (DEXA) analysis, intravenous glucose tolerance tests (GTTs), and determination of fasting glucose and insulin levels were performed before necropsy, as described [10]. For DEXA studies, monkeys were sedated with ketamine and

positioned supine on the bed of a Hologic DEXA scanner (Discovery scanner, Hologic Inc., Bedford, MA, USA). Two to three scans were performed for each animal and averages were calculated for each measure. For glucose tolerance tests (GTTs), animals were fasted overnight, sedated with Telazol and a glucose bolus (50% dextrose solution) administered at a dose of 0.6 g/kg via the saphenous vein. Baseline blood samples were obtained prior to the glucose injection, and 1-ml blood samples were taken at 1, 3, 5, 10, 20, 40 and 60 min later by venipuncture. Glucose was measured immediately using a OneTouch Ultra Blood Glucose Monitor (LifeScan), and the remainder of the blood was placed in heparinized tubes on ice for insulin assay. Homeostatic Model Assessment of Insulin Resistance (HOMA-IR) was calculated as fasting serum insulin (μU/ml) × fasting plasma glucose (mg/dl)/405.

Hormone assays

Insulin was analyzed in the ONPRC Endocrine Technologies Core by immunoassay on a Roche cobas e411 chemiluminescence-based automated immunoassay platform (Roche Diagnostics, Indianapolis, IN). The assay range was 0.2–1000 μIU/ml. Intra-assay CV was 1.1%. Inter-assay CV for the insulin assay is 3.7%. Testosterone was analyzed by immunoassay on a Roche cobas e411 chemiluminescence-based automated immunoassay platform (Roche Diagnostics, Indianapolis, IN). The assay range was 0.025–15 ng/ml. Intra-assay CV was 2.2%. Inter-assay CV for the testosterone assay is 6.7%. Chemokine ligand 5 (CCL5) was analyzed by ELISA following the manufacturer's instructions (R&D Systems, Minneapolis, MN). Samples were diluted 1:100 prior to analysis. The assay range was 31.3–2000 pg/ml; intra-assay CV was 3.5%. Inter-assay CV for the CCL5 ELISA is 5.7%. C-reactive peptide (CRP) was analyzed by ELISA following the manufacturer's instructions (ALPCO Diagnostics, Salem, NH). Samples were diluted 1:100 prior to analysis. The assay range was 0.95–150 ng/ml. Intra-assay CV was 4.3%. Inter-assay CV for the CRP ELISA is 14.8%.

WAT histology and image analysis

WAT histology and image analysis were performed as described [11]. Briefly, 200 to 500-mg fragments of subcutaneous (SC)-WAT and OM-WAT were collected at necropsy and fixed in zinc formalin (Fisher Scientific, Hampton, NH, USA) at 4°C for 48 hours. Samples were transferred to 70% (v/v) ethanol for 5 days, embedded in Paraplast wax (Leica, Wetzlar, Germany), and 5-μm sections were prepared using a micron rotary microtome. Slides were stained with Picrosirius red Stain Kit (Abcam, Boston, MA, USA) according to the manufacturer's instructions. Images representing tissue segments of approximately 5 to 10 mm in size were acquired using an Aperio AT2 System slide scanner (Leica Biosystems, Wetzlar, Germany) and saved as gigabyte-size TIFF files. The mean area of adipocytes and fibrotic fraction (the proportion of Picrosirius red-positive staining per WAT section) were measured using the thresholding function of Image J, resulting in foreground (Picrosirius red-positive) and background (Picrosirius red-negative) pixels within each section. Specific WAT parameters are shown in Supplementary Table 1.

Cell isolation and cryopreservation

All tissues were collected and cells isolated using the following protocol on the day of necropsy unless stated otherwise. Five grams of OM-WAT were collected at necropsy and

transported to the lab in 25 mL ice-cold FACS buffer (DPBS (Thermofisher, Waltham, MA, USA) containing 0.5% BSA (Sigma-Aldrich, St. Louis, MO, USA) and 2 mM EDTA (Sigma-Aldrich)). Tissue was minced in a 6-well dish and transferred to 10 mL of freshly-made, filter-sterilized collagenase solution (120 mg collagenase type-II (Gibco, cat#17101–015), 1.4 g BSA (Sigma-Aldrich), DPBS to 40 mL, and 80 μL 1 M $CaCl_2$). Tissue was digested for 30–40 min, while vortexed every 5 min until tissue clumps were dissolved. Ice-cold FACS buffer (40 mL) was added to the digested tissue and the cell suspension was filtered through a 100-micron cell strainer. The tube was centrifuged at 1500 rpm (400 × g) for 10 min at 4ºC, and the supernatant was discarded. 5 mL red-blood-lysis (RBC) buffer was added to the cell pellet and incubated for 8 min at room temperature. The cell pellet was washed in ice-cold FACS buffer two more times by centrifugation at 1500 rpm for 10 min at 4ºC and resuspended in 1 mL FACS buffer on ice for cell counting. Cells were centrifuged and the supernatant was replaced with 1–2 mL ice-cold CryoStor CS10 (STEMCELL Technologies, Vancouver, BC, Canada). Cells were gently resuspended and cryopreserved in 2–4 aliquots at −80ºC for 24h and then stored in liquid N_2 until immune cell analyses.

Femoral bone marrow (FBM) was removed by flashing the femur with 20 mL ice-cold FACS buffer. FBM was gently disrupted using a 25-ml syringe loaded with a blunt needle, and the cell suspension was filtered through a 100-μm cell strainer. The cell suspension was centrifuged for 10 min at 1500 rpm and the pellet was resuspended and incubated for 8 min at room temperature in the RBC buffer. Cells were washed and cryopreserved as described above. Vertebral BM was extracted from the T12 vertebra using a bone cutter and a ceramic mortar and pestle. BM cell suspensions were then filtered through a 100-micron cell strainer and processed as described for FBM.

Reproductive tract and ovaries from rhesus macaques were obtained at necropsy, submerged in Hanks Balanced Salt solution and delivered to the lab within 15 minutes. For END isolation, the uterus was bisected along the longitudinal axis from the fundus to the cervix and then further divided into quarters. Full-thickness tissue sections (~5 mm) extending from the uterine lumen to the outer myometrium were biopsied from each quarter. OV were isolated from the reproductive tract, trimmed free of fat, and bisected. The CL was removed from the dominant ovary by use of curved dissecting scissors. END, CL and OV cell suspensions were then generated using the same collagenase digestion method described above and cryopreserved until immune cell analyses.

LNs were collected into ice-cold FACS buffer, diced with scalpels, mashed through a 70-μm filter, and processed for cell isolation as described for WAT. Blood samples were collected in EDTA-treated tubes and peripheral blood mononuclear cells (PBMCs) were isolated by centrifugation at 2000 rpm (800 × g) for 30 min using a Lymphoprep gradient (STEMCELL Technologies) as described [21].

Flow cytometry

Cryopreserved cells were washed and analyzed by flow cytometry using monoclonal antibodies previously validated for specific binding to rhesus macaque antigens [17] and positive/negative cells were detected using lymphoid-specific and myeloid-specific gating

strategies. For lymphoid staining, 5×10^5-1×10^6 cells were incubated with a custom antibody panel that included anti-CD45 (D058–1283, Biolegend, San Diego, USA), anti-CD3 (clone SP34, BD Pharmingen, Franklin Lakes, NJ, USA), anti-CD4 (clone L200, BD Pharmingen), anti-CD8 (clone SK1, Biolegend), anti-HLA-DR (clone L243, Biolegend), anti-CD25 (clone 2A3, BD Pharmingen), anti-FoxP3 (clone PCH101, Thermofisher, Waltham, MA, USA), anti-CD28 (clone CD28.2, Biolegend), anti-Ki67 (clone B56, BD Biosciences), and fixable amine-reactive dye (Invitrogen, Waltham, MA, USA). For macrophage staining, 5×10^5-1×10^6 cells were incubated with a custom antibody panel that included anti-CD45 (D058–1283, Biolegend), anti-CD123 (clone 6H6, Biolegend), anti-HLA-DR (clone L243, Biolegend), anti-CD11b (clone ICRF44, Biolegend), anti-CD163 (clone GHI/61, Biolegend), and anti-CD11c (clone 3.9, Biolegend) and fixable amine-reactive dye (Invitrogen). For lineage-negative staining, anti-CD3 (clone SP34, BD Pharmingen), anti-CD8 (clone SK1, Biolegend), and anti-CD20 (clone 2H7, Biolegend) were included in a separate panel. All cell aliquots were incubated with these aforementioned antibodies (at the manufacturer's suggested dilution) for 30 minutes at 4ºC, then non-specific binding was reduced by washing twice with PBS containing 2% FBS before fluorescence detection. Fluorescence intensity was acquired using an LSRII flow cytometer (BD Biosciences). Data were then analyzed using FlowJo v10 (Tree Star, Ashland, OR, USA) and Prism v6 (GraphPad Software, San Diego, CA, USA).

Functional responses in FBM and T12 macrophages were evaluated as described [21]. Specifically, 5×10^5 BM cells were stimulated with LPS (TLR4 agonist 1 μg/mL), Pam3CSK4 (TLR1/2 agonist, 1 μg/mL), or HKLM (TLR2 agonist, 108 particles/mL) for 8 h in the presence of 5 μg/mL brefeldin A (Sigma-Aldrich). TLR agonists were purchased from InvivoGen (San Diego, CA, USA). Cells were stained with antibodies to CD11b and HLA-DR to delineate monocytes/macrophages. Following surface staining, cells were permeabilized using the Foxp3/Transcription Factor Staining Buffer Set (eBioscience, cat# 00–5523-00) and stained with monoclonal antibodies TNFα, (clone MAb11, Invitrogen) and IL-6 (clone MQ2–6A3, BD Biosciences). Samples were washed twice with PBS containing 2% FBS and analyzed on an LSRII flow cytometer as described above.

Statistical analysis

All statistical analyses were conducted in Excel and Prism 8 (GraphPad). Anatomical and metabolic parameters were compared using a two-tailed unpaired t-test. A correlation analysis was conducted by calculating the Pearson correlation coefficients and their associated p-values. Flow cytometry data analysis across multiple tissues and animal groups were conducted using 2-way ANOVA and a Bonferroni's multiple comparisons test.

Results

Effects of T+WSD treatment on metabolic parameters and pro-inflammatory mediators

To assess the effects of T+WSD treatment on metabolic parameters, we determined body composition by DEXA and glucose tolerance by GTT. Animals treated with T+WSD for one year exhibited greater levels of circulating T, a significantly greater percentage of total body fat, and greater fasting insulin and glucose concentrations than control animals

(Table 1). T+WSD animals were also more insulin resistant than control animals, based on higher Homeostatic Model Assessment for Insulin Resistance (HOMA-IR) values, and more glucose intolerant, based on greater Area Under Curve (AUC) glucose values measured by GTT (Table 1). We next assessed the effects of T+WSD on systemic pro-inflammatory mediators. Circulating levels of the proinflammatory mediators CRP and CCL5 were not significantly different between the control and T+WSD groups (Table 1). Collectively, our data indicate that a one-year T+WSD treatment results in a significant increase in body fat and glucose intolerance, but has no significant effect on the levels of systemic proinflammatory markers in adult female rhesus macaques.

Effects of T+WSD treatment on WAT morphological parameters

To determine whether T+WSD treatment selectively modulates depot-specific morphological characteristics of WAT, we performed histological staining of WAT sections using picrosirius red and analyzed adipocyte size and tissue fibrosis. The mean areas of OM and subcutaneous (SC) adipocytes were significantly higher in T+WSD-treated animals compared to control animals (Figure 1B and C; Supplementary Table 1). Additionally, the fibrotic fractions in OM-WAT and SC-WAT were not significantly different between the groups (Figure 1B and D; Supplementary Table 1). These data show that T+WSD treatment of young adult female rhesus macaques led to the development of adipocyte hypertrophy without overt fibrosis. Furthermore, the mean area of OM adipocytes and body fat content were positively correlated with circulating T levels (Figure 1E and F). Collectively, these results are consistent with our previous studies showing similar metabolic (obesity and insulin resistance) and adipose-specific (adipocyte hypertrophy) phenotypes in female macaques exposed at puberty to the combination of T and WSD [9–12].

Effects of T+WSD treatment on tissue-resident macrophages

We next investigated whether T+WSD was associated with higher proinflammatory responses in tissue-resident macrophages using flow cytometry, which provided detailed insight into tissue-specific immune phenotypes. Cells residing in nonlymphoid tissues (OM-WAT, CL, OV, ENDO, and FBM) were stained with a myeloid-specific antibody panel. Our analysis revealed that T+WSD treatment had no significant effect on the frequencies of macrophages (CD45+HLADR+CD11b+) in the tissues examined. Additionally, we found no significant group differences in frequencies of proinflammatory M1-like macrophages (HLADR+CD11b+CD163-CD11c+) [22–24], anti-inflammatory M2-like macrophages (HLADR+CD11b+CD163+CD11c-) [25–28], or mixed M1/M2 macrophages (HLADR+CD11b+CD163+CD11c+) [24,29] in all tissues examined (Figure 2). Collectively, our results indicate that macrophage polarization is not significantly affected by T+WSD treatment.

To test whether T+WSD treatment impacts macrophage function, we measured cytokine responses of macrophages residing in OM-WAT and BM (including FBM and T12) to toll-like receptor (TLR) agonists in vitro. Cell mixtures were incubated with LPS (TLR4 agonist), Pam3CSK4 (TLR1/2 agonist), or HKLM (TLR2 agonist) in the presence of brefeldin A to enhance intracellular cytokine staining signals by blocking transport processes during cell activation. Cells were stained with antibodies to CD11b and HLA-DR

to delineate monocytes/macrophages. Following surface staining, cells were permeabilized and stained with monoclonal antibodies to TNFα and IL-6 and analyzed by flow cytometry (Figure 3A and B). Because OM-WAT cells showed poor recovery following this procedure, we focused on the functional analysis of macrophages residing in FBM and T12 marrow. FBM and T12 macrophages showed variable TNF responses to different TLR agonists, while no significant group differences in TLR responses were observed (Figure 3D and E). Interestingly, IL-6 responses of BM macrophages to different TLR ligands were attenuated by T+WSD treatment, particularly in the FBM compartment (Figure 3F and G). These data suggest that T+WSD treatment does not enhance TLR-mediated proinflammatory responses, but may induce immune tolerance in BM macrophages.

Effects of T+WSD treatment on tissue-resident lymphocytes

We next investigated whether T+WSD treatment is associated with higher proinflammatory responses in tissue-resident lymphoid cells. Cells residing in nonlymphoid and lymphoid tissues (OM-WAT, CL, OV, ENDO, FBM, and LNs) and PBMC were stained with a lymphoid-specific antibody panel. Our analysis of lymphoid subsets showed no significant group differences in frequencies of CD4+, CD8+, and CD4+CD8+ T cells in all tissues examined (Supplementary Figures S1A–E). We next determined whether T+WSD treatment affected tissue-resident Tregs, (CD3+CD4+CD25+FoxP3+) reported to play a role in the pathogenesis of obesity and insulin resistance [30–32]. However, we observed no differences in the frequencies of Tregs [33] in all tissues examined between control and T+WSD-treated animals (Supplementary Figures S1A and F).

We next analyzed tissue-resident memory CD4+ and CD8+ T-cells. To discriminate between different memory T-cell subsets, CD8+ and CD4+ cells were co-stained with CD28 and CD95 antibodies to delineate CD28+CD95- naïve (Tn), CD28+CD95+ central memory (Tcm), and CD28- effector memory (Tem)/effector (Teff) T-cells (Figures 4A and B; Supplementary Figure S2A). We found that CD28- T-cells did not express CD25 or the activation marker HLA-DR, suggesting that CD28- cells residing in OM-WAT are primarily composed of Tem in both control and treated groups (Figures 4E and F). T+WSD treatment resulted in a significant reduction in the frequencies of CD8+ Tem in OM-WAT, but not in other tissues or PBMCs (Figure 4G) and had no significant effect on frequencies of CD4+ memory subsets (Supplementary Figures 2B and C). We found no significant group differences in frequencies of proliferating Tems in the tissues examined (Figures 4A, B, and H). However, the frequencies of proliferating Tems in OM-WAT were negatively correlated with HOMA-IR (Figure 4I). To test whether T+WSD treatment accelerates T cell exhaustion, we analyzed the levels of Programmed Cell Death Ligand 1 (PD-1) in Tems. Tems from control and treated animals expressed very low levels of PD-1 (Figures 4A and B, right panels). In contrast, T12 CD8+ Tems expressed low but detectable levels of PD-1 and low levels of Ki67 (Figures 4C and D), which validated our PD-1 staining in NHPs. These results suggest that T-cell exhaustion is not involved in the decline in CD8+ Tems in OM-WAT of T+WSD-treated animals.

Correlations between metabolic and immune parameters

Notably, CD8+ Tem frequencies in OM-WAT were negatively correlated with HOMA-IR, fasting insulin, fasting glucose, glucose AUC, and % body fat (Figure 4J and Table 2). In contrast, Tcm frequencies in OM-WAT were positively correlated with HOMA-IR (Figure 4K), while the frequencies of Tn in OM-WAT were not correlated with HOMA-IR (Figure 4L). Additionally, CD4+ Tem and M1 macrophage frequencies in OM-WAT were not correlated with any of the parameters examined (Table 2).

Discussion

While the pathogenesis of PCOS is not fully understood, androgen excess, insulin resistance, adipocyte hypertrophy and low-grade inflammation can form a vicious cycle interconnecting metabolic and reproductive disarrangements in women with PCOS [4,6,8]. However, whether androgen excess and adipocyte hypertrophy alone can trigger a systemic and tissue-resident proinflammatory milieu remains to be defined. Here, we demonstrate that the combination of hyperandrogenemia and obesogenic WSD are not sufficient for inducing a proinflammatory phenotype after one year of treatment, suggesting that additional factors or a longer treatment period are required for immune cell activation in this experimental model.

In the present study, we found that one year of exposure to hyperandrogenemia in the presence of WSD (T+WSD) induces obesity, glucose intolerance, insulin resistance, and adipocyte hypertrophy. Numerous studies in PCOS patients and in animal models of PCOS have shown that androgen excess is associated with metabolic abnormalities, including insulin resistance, obesity, and adipocyte hypertrophy [11,34–39]. The data presented here are also in line with our previous studies showing that T+WSD exposure for three years, starting at puberty, induced metabolic dysfunction and OM-WAT hypertrophy in female rhesus macaques [9–11]. Specifically, T+WSD treatment accelerated the development of WAT dysfunction through androgen-specific suppression of lipolysis and WSD-specific reduction in WAT capillary density [9,11]. In the same studies, exposure to T or WSD alone for three years, starting at puberty, did not induce adipocyte hypertrophy but did exert negative effects on some functional characteristics of WAT [9,11]. However, the effects of WSD or T alone on metabolic and WAT characteristics were not examined in the present study because our previous results demonstrated that the combination of T and WSD was required for the development of more severe metabolic effects.

Here, we also report that T+WSD treatment was not associated with elevated levels of the pro-inflammatory mediators CRP and CCL5. In contrast, previous studies have shown that PCOS patients exhibit elevated markers of systemic inflammation, including CRP [40], IL6, and TNFα [41,42]. CCL5 levels in the blood and visceral WAT have been shown to be elevated in letrozole-induced PCOS in mice and in PCOS patients [43,44]. Our previous study showed that T+WSD treatment or the consumption of WSD alone for three years was associated with elevated CRP levels in female rhesus macaques [10], suggesting that longer treatment is necessary for inducing a systemic proinflammatory response in NHPs.

One surprising finding of the present study was the lack of macrophage proinflammatory activation despite developing obesity, adipocyte hypertrophy, and insulin resistance in T+WSD-treated animals. Specifically, we found no evidence of macrophage tissue recruitment and proinflammatory polarization toward the classically activated M1 phenotype in all tissues examined, including OM-WAT, CL, OV, END, and BM. Furthermore, the frequencies of anti-inflammatory, alternatively activated M2 and mixed M1/M2 macrophages were not affected by T+WSD. Obesity has been shown to be associated with accumulation of proinflammatory macrophages in rodent [23,28,45–50] and human [22,24,29,51] WAT, based principally on immunohistochemistry. However, several subsequent studies using qPCR and immunohistochemistry as well as flow cytometry analyses similar to our study, showed that human obesity is not associated with proinflammatory M1 polarization in WAT [52–55]. In addition to our flow cytometry data showing that obesity in macaques is not associated with M1 polarization. Additionally, our functional data, using BM macrophages, further support the idea that T+WSD treatment is not associated with enhanced classical macrophage activation. Specifically, BM macrophages from the T+WSD and control groups produced similar amounts of TNFα in response to LPS and other TLR ligands. Interestingly, IL6 production by FBM macrophages in response to LPS (TLR4 agonist) and HKLM (TLR2 agonist) stimulation was significantly blunted by T+WSD treatment compared to control treatment, suggesting the potential development of immune tolerance to different TLR agonists in response to T+WSD. Further studies are needed to elucidate whether T+WSD and WSD and T alone modulates macrophage activation in other peripheral tissues.

We also analyzed lymphoid immune cells residing in peripheral tissues and PBMCs and found that the frequencies of the major subsets of T cells, including Treg, were not affected by treatment. Treg cells play a role in the pathogenesis of obesity and insulin resistance and Treg frequencies are reduced in PCOS patients [56,57]. Recent studies have shown that obesity can alter the properties of WAT-resident T cells prior to activation of macrophages [58–64]. Specifically, effector $CD8^+$ T-cells residing in WAT have been suggested to initiate a proinflammatory response leading to the accumulation of proinflammatory macrophages in WAT [65,66]. In contrast, in present study, short-term T+WSD treatment was not associated with proinflammatory T-cell activation in any of the tissues examined.

Here, we also addressed the potential alteration of immune cell composition in reproductive organs. OM-WAT is a major human visceral fat depot associated with multiple abdominal organs, including the reproductive tract and lymphoid tissues. Therefore, changes in the local immune milieu in WAT may also affect the local immune composition of reproductive tissues. Immune cell composition is dynamic in reproductive tissues and is thought to play an important role in normal processes important for fertility [4,67]. For example, the primate CL undergoes significant changes in immune cell content during its development and regression at the end of the menstrual cycle [68,69]. Uterine immune cells are thought to play an important role in the process of embryo implantation [70,71]. There were no immunophenotypic changes detected in uterine and regional lymphoid tissues following T+WSD treatment. Collectively, our study indicates that short-term exposure to an obesogenic diet and mild hyperandrogenemia is not sufficient for inducing proinflammatory conditions.

In the present study, we also studied the effect of T+WSD treatment on tissue-resident T-cells implicated in immunological memory formation. OM-WAT plays an active role in metabolism and regulation of immune responses to antigens [72,73]. Recent studies show that obesity and type 2 diabetes can alter CD8+ T-cell responses against viral infection and cancer [58,74–76]. The development of immunological dysfunction of WAT-resident T-cells has been reported in obese subjects [77–80]. However, the tissue-resident immune cell phenotypes of obese females with hyperandrogenemia remains poorly understood. We found that the frequencies of Tem were significantly reduced in OM-WAT of T+WSD-treated animals. Intriguingly, frequencies of WAT-resident Treg cells were inversely correlated with HOMA-IR, fasting insulin, fasting glucose, glucose AUC, and body fat, suggesting that metabolic dysfunction has a negative impact on the proliferating pool of Tem. In summary, our study demonstrates an intriguing connection between T+WSD-induced obesity and a decline in CD8+ Tem in OM-WAT, and warrants future studies addressing the role of T, insulin and other metabolic factors in regulating Tem differentiation and function in health and PCOS.

Our study has several limitations. (1) The small sample size may have limited our power to detect smaller tissue-specific effects of T+WSD on immune cell subsets. (2) The higher number of animals recruited to the T+WSD group compared to the control group was dictated by the experimental design of this study. Specifically, additional T+WSD animals were initially generated to compensate for potential animal loss due to endometriosis, as our earlier studies demonstrated that long-term T+WSD treatment resulted in earlier onset and more severe types of endometriosis [81]. However, none of the animals treated with T+WSD for one year developed endometriosis, suggesting that longer treatment and/or animal age can influence disease progression. (3) The effects of short-term T+WSD treatment on reproductive phenotypes are not included here and will be reported in the separate study (manuscript in preparation). In our previous studies, long-term T+WSD treatment did not result in anovulatory cycles, but did result in ovarian and uterine dysfunction, leading to reduced fertility [12,13]. While long-term exposure to (experimentally induced) hyperandrogenemia and WSD increased the number of antral follicles [12], it is clear that long-term and particularly short-term T+WSD regomens do not fully recapitulate all aspects of PCOS. (4) The present study did not examine the effects of T or WSD alone on immune cell characteristics and highlights the need to better discriminate the effects of WSD versus excess T on the immune system. (5) While the functional significance of WAT-resident Tems remains to be determined, it is possible that WAT forms a unique reservoir for pathogen-responsive Tems and that Tem responses to specific pathogens are modulated by obesity [82].

Supplementary Material

Refer to Web version on PubMed Central for supplementary material.

Acknowledgments

This study was supported by NIH grants P50 HD071836 to CTR and P51 OD01192 for operation of the Oregon National Primate Research Center. We also acknowledge the assistance of the ONPRC Endocrine Technologies Core. We would like to thank Dr. Paul Kievit for critical review of the manuscript.

References

1. Dumesic DA, Goodarzi MO, Chazenbalk GD, Abbott DH. Intrauterine environment and polycystic ovary syndrome. Semin Reprod Med. 2014;32(3):159–165. [PubMed: 24715510]
2. Goodarzi MO, Dumesic DA, Chazenbalk G, Azziz R. Polycystic ovary syndrome: etiology, pathogenesis and diagnosis. Nat Rev Endocrinol. 2011.
3. Azziz R, Carmina E, Dewailly D, et al. The Androgen Excess and PCOS Society criteria for the polycystic ovary syndrome: the complete task force report. Fertil Steril. 2009;91(2):456–488. [PubMed: 18950759]
4. Hu C, Pang B, Ma Z, Yi H. Immunophenotypic Profiles in Polycystic Ovary Syndrome. Mediators Inflamm. 2020;2020:5894768. [PubMed: 32256193]
5. Qi X, Zhang B, Zhao Y, et al. Hyperhomocysteinemia Promotes Insulin Resistance and Adipose Tissue Inflammation in PCOS Mice Through Modulating M2 Macrophage Polarization via Estrogen Suppression. Endocrinology. 2017;158(5):1181–1193. [PubMed: 28323956]
6. Spritzer PM, Lecke SB, Satler F, Morsch DM. Adipose tissue dysfunction, adipokines, and low-grade chronic inflammation in polycystic ovary syndrome. Reproduction. 2015;149(5):R219–227. [PubMed: 25628442]
7. Thomann R, Rossinelli N, Keller U, et al. Differences in low-grade chronic inflammation and insulin resistance in women with previous gestational diabetes mellitus and women with polycystic ovary syndrome. Gynecol Endocrinol. 2008;24(4):199–206. [PubMed: 18382906]
8. Rocha AL, Oliveira FR, Azevedo RC, et al. Recent advances in the understanding and management of polycystic ovary syndrome. F1000Res. 2019;8. [PubMed: 30854195]
9. Carbone L, Davis BA, Fei SS, et al. Synergistic Effects of Hyperandrogenemia and Obesogenic Western-style Diet on Transcription and DNA Methylation in Visceral Adipose Tissue of Nonhuman Primates. Sci Rep. 2019;9(1):19232. [PubMed: 31848372]
10. True CA, Takahashi DL, Burns SE, et al. Chronic combined hyperandrogenemia and western-style diet in young female rhesus macaques causes greater metabolic impairments compared to either treatment alone. Hum Reprod. 2017;32(9):1880–1891. [PubMed: 28854721]
11. Varlamov O, Bishop CV, Handu M, et al. Combined androgen excess and Western-style diet accelerates adipose tissue dysfunction in young adult, female nonhuman primates. Hum Reprod. 2017;32(9):1892–1902. [PubMed: 28854720]
12. Bishop CV, Mishler EC, Takahashi DL, et al. Chronic hyperandrogenemia in the presence and absence of a western-style diet impairs ovarian and uterine structure/function in young adult rhesus monkeys. Hum Reprod. 2018;33(1):128–139. [PubMed: 29190387]
13. Bishop CV, Stouffer RL, Takahashi DL, et al. Chronic hyperandrogenemia and western-style diet beginning at puberty reduces fertility and increases metabolic dysfunction during pregnancy in young adult, female macaques. Hum Reprod. 2018;33(4):694–705. [PubMed: 29401269]
14. Yu VW, Scadden DT. Heterogeneity of the bone marrow niche. Curr Opin Hematol. 2016;23(4):331–338. [PubMed: 27177311]
15. Pinho S, Frenette PS. Haematopoietic stem cell activity and interactions with the niche. Nat Rev Mol Cell Biol. 2019.
16. Sureshchandra S, Chan CN, Robino JJ, et al. Maternal Western-style diet remodels the transcriptional landscape of fetal hematopoietic stem and progenitor cells in rhesus macaques. Stem Cell Reports. 2022.
17. Burwitz BJ, Reed JS, Hammond KB, et al. Technical advance: liposomal alendronate depletes monocytes and macrophages in the nonhuman primate model of human disease. J Leukoc Biol. 2014;96(3):491–501. [PubMed: 24823811]
18. Carmina E, Chu MC, Longo RA, Rini GB, Lobo RA. Phenotypic variation in hyperandrogenic women influences the findings of abnormal metabolic and cardiovascular risk parameters. J Clin Endocrinol Metab. 2005;90(5):2545–2549. [PubMed: 15728203]
19. Azziz R, Carmina E, Dewailly D, et al. Positions statement: criteria for defining polycystic ovary syndrome as a predominantly hyperandrogenic syndrome: an Androgen Excess Society guideline. J Clin Endocrinol Metab. 2006;91(11):4237–4245. [PubMed: 16940456]

20. Abbott DH, Dumesic DA, Levine JE. Hyperandrogenic origins of polycystic ovary syndrome - implications for pathophysiology and therapy. Expert Rev Endocrinol Metab. 2019;14(2):131–143. [PubMed: 30767580]
21. Sureshchandra S, Doratt BM, Mendza N, et al. Maternal obesity blunts antimicrobial responses in fetal monocytes. Elife. 2023;12.
22. Wouters K, Gaens K, Bijnen M, et al. Circulating classical monocytes are associated with CD11c(+) macrophages in human visceral adipose tissue. Sci Rep. 2017;7:42665. [PubMed: 28198418]
23. Nguyen MT, Favelyukis S, Nguyen AK, et al. A subpopulation of macrophages infiltrates hypertrophic adipose tissue and is activated by free fatty acids via Toll-like receptors 2 and 4 and JNK-dependent pathways. J Biol Chem. 2007;282(48):35279–35292. [PubMed: 17916553]
24. Wentworth JM, Naselli G, Brown WA, et al. Pro-inflammatory CD11c+CD206+ adipose tissue macrophages are associated with insulin resistance in human obesity. Diabetes. 2010;59(7):1648–1656. [PubMed: 20357360]
25. Michaud A, Tordjman J, Pelletier M, et al. Relevance of omental pericellular adipose tissue collagen in the pathophysiology of human abdominal obesity and related cardiometabolic risk. Int J Obes (Lond). 2016;40(12):1823–1831. [PubMed: 27698346]
26. Carestia A, Mena HA, Olexen CM, et al. Platelets Promote Macrophage Polarization toward Pro-inflammatory Phenotype and Increase Survival of Septic Mice. Cell Rep. 2019;28(4):896–908 e895. [PubMed: 31340152]
27. Poledne R, Kralova Lesna I, Kralova A, Fronek J, Cejkova S. The relationship between non-HDL cholesterol and macrophage phenotypes in human adipose tissue. J Lipid Res. 2016;57(10):1899–1905. [PubMed: 27481939]
28. Shaul ME, Bennett G, Strissel KJ, Greenberg AS, Obin MS. Dynamic, M2-like remodeling phenotypes of CD11c+ adipose tissue macrophages during high-fat diet--induced obesity in mice. Diabetes. 2010;59(5):1171–1181. [PubMed: 20185806]
29. Nakajima S, Koh V, Kua LF, et al. Accumulation of CD11c+CD163+ Adipose Tissue Macrophages through Upregulation of Intracellular 11beta-HSD1 in Human Obesity. J Immunol. 2016;197(9):3735–3745. [PubMed: 27698011]
30. van der Weerd K, Dik WA, Schrijver B, et al. Morbidly obese human subjects have increased peripheral blood CD4+ T cells with skewing toward a Treg- and Th2-dominated phenotype. Diabetes. 2012;61(2):401–408. [PubMed: 22228716]
31. Feuerer M, Herrero L, Cipolletta D, et al. Lean, but not obese, fat is enriched for a unique population of regulatory T cells that affect metabolic parameters. Nat Med. 2009;15(8):930–939. [PubMed: 19633656]
32. Eller K, Kirsch A, Wolf AM, et al. Potential role of regulatory T cells in reversing obesity-linked insulin resistance and diabetic nephropathy. Diabetes. 2011;60(11):2954–2962. [PubMed: 21911743]
33. Arruvito L, Sanz M, Banham AH, Fainboim L. Expansion of CD4+CD25+and FOXP3+ regulatory T cells during the follicular phase of the menstrual cycle: implications for human reproduction. J Immunol. 2007;178(4):2572–2578. [PubMed: 17277167]
34. Corton M, Botella-Carretero JI, Benguria A, et al. Differential gene expression profile in omental adipose tissue in women with polycystic ovary syndrome. J Clin Endocrinol Metab. 2007;92(1):328–337. [PubMed: 17062763]
35. Dumesic DA, Phan JD, Leung KL, et al. Adipose Insulin Resistance in Normal-Weight Polycystic Ovary Syndrome Women. J Clin Endocrinol Metab. 2019.
36. Lu C, Cardoso RC, Puttabyatappa M, Padmanabhan V. Developmental Programming: Prenatal Testosterone Excess and Insulin Signaling Disruptions in Female Sheep. Biol Reprod. 2016;94(5):113. [PubMed: 27053365]
37. Caldwell AS, Middleton LJ, Jimenez M, et al. Characterization of reproductive, metabolic, and endocrine features of polycystic ovary syndrome in female hyperandrogenic mouse models. Endocrinology. 2014;155(8):3146–3159. [PubMed: 24877633]
38. Manneras-Holm L, Leonhardt H, Kullberg J, et al. Adipose tissue has aberrant morphology and function in PCOS: enlarged adipocytes and low serum adiponectin, but not circulating sex steroids,

are strongly associated with insulin resistance. J Clin Endocrinol Metab. 2011;96(2):E304–311. [PubMed: 21084397]

39. Ciaraldi TP, Aroda V, Mudaliar S, Chang RJ, Henry RR. Polycystic ovary syndrome is associated with tissue-specific differences in insulin resistance. J Clin Endocrinol Metab. 2009;94(1):157–163. [PubMed: 18854391]
40. Boulman N, Levy Y, Leiba R, et al. Increased C-reactive protein levels in the polycystic ovary syndrome: a marker of cardiovascular disease. J Clin Endocrinol Metab. 2004;89(5):2160–2165. [PubMed: 15126536]
41. Amato G, Conte M, Mazziotti G, et al. Serum and follicular fluid cytokines in polycystic ovary syndrome during stimulated cycles. Obstet Gynecol. 2003;101(6):1177–1182. [PubMed: 12798522]
42. Manneras L, Jonsdottir IH, Holmang A, Lonn M, Stener-Victorin E. Low-frequency electro-acupuncture and physical exercise improve metabolic disturbances and modulate gene expression in adipose tissue in rats with dihydrotestosterone-induced polycystic ovary syndrome. Endocrinology. 2008;149(7):3559–3568. [PubMed: 18388196]
43. Seow KM, Liu PS, Chen KH, et al. Cysteine-Cysteine Motif Chemokine Receptor 5 Expression in Letrozole-Induced Polycystic Ovary Syndrome Mice. Int J Mol Sci. 2021;23(1).
44. Juan CC, Chen KH, Chen CW, et al. Increased regulated on activation, normal T-cell expressed and secreted levels and cysteine-cysteine chemokine receptor 5 upregulation in omental adipose tissue and peripheral blood mononuclear cells are associated with testosterone level and insulin resistance in polycystic ovary syndrome. Fertil Steril. 2021;116(4):1139–1146. [PubMed: 34119324]
45. Kitade H, Sawamoto K, Nagashimada M, et al. CCR5 plays a critical role in obesity-induced adipose tissue inflammation and insulin resistance by regulating both macrophage recruitment and M1/M2 status. Diabetes. 2012;61(7):1680–1690. [PubMed: 22474027]
46. Xu H, Barnes GT, Yang Q, et al. Chronic inflammation in fat plays a crucial role in the development of obesity-related insulin resistance. J Clin Invest. 2003;112(12):1821–1830. [PubMed: 14679177]
47. McCurdy CE, Schenk S, Holliday MJ, et al. Attenuated Pik3r1 expression prevents insulin resistance and adipose tissue macrophage accumulation in diet-induced obese mice. Diabetes. 2012;61(10):2495–2505. [PubMed: 22698915]
48. Averill MM, Barnhart S, Becker L, et al. S100A9 differentially modifies phenotypic states of neutrophils, macrophages, and dendritic cells: implications for atherosclerosis and adipose tissue inflammation. Circulation. 2011;123(11):1216–1226. [PubMed: 21382888]
49. Ye J, Gao Z, Yin J, He Q. Hypoxia is a potential risk factor for chronic inflammation and adiponectin reduction in adipose tissue of ob/ob and dietary obese mice. Am J Physiol Endocrinol Metab. 2007;293(4):E1118–1128. [PubMed: 17666485]
50. Lumeng CN, DelProposto JB, Westcott DJ, Saltiel AR. Phenotypic switching of adipose tissue macrophages with obesity is generated by spatiotemporal differences in macrophage subtypes. Diabetes. 2008;57(12):3239–3246. [PubMed: 18829989]
51. Liu LF, Kodama K, Wei K, et al. The receptor CD44 is associated with systemic insulin resistance and proinflammatory macrophages in human adipose tissue. Diabetologia. 2015;58(7):1579–1586. [PubMed: 25952479]
52. Martinez FO, Gordon S. The M1 and M2 paradigm of macrophage activation: time for reassessment. F1000Prime Rep. 2014;6:13. [PubMed: 24669294]
53. Fjeldborg K, Pedersen SB, Moller HJ, Christiansen T, Bennetzen M, Richelsen B. Human adipose tissue macrophages are enhanced but changed to an anti-inflammatory profile in obesity. J Immunol Res. 2014;2014:309548. [PubMed: 24741586]
54. Blaszczak AM, Jalilvand A, Liu J, et al. Human Visceral Adipose Tissue Macrophages Are Not Adequately Defined by Standard Methods of Characterization. J Diabetes Res. 2019;2019:8124563. [PubMed: 30719456]
55. Espinosa De Ycaza AE, Sondergaard E, Morgan-Bathke M, et al. Adipose Tissue Inflammation Is Not Related to Adipose Insulin Resistance in Humans. Diabetes. 2022;71(3):381–393. [PubMed: 34857544]

56. Nasri F, Doroudchi M, Namavar Jahromi B, Gharesi-Fard B. T Helper Cells Profile and CD4+CD25+Foxp3+Regulatory T Cells in Polycystic Ovary Syndrome. Iran J Immunol. 2018;15(3):175–185. [PubMed: 30246693]
57. Krishna MB, Joseph A, Subramaniam AG, Gupta A, Pillai SM, Laloraya M. Reduced Tregs in peripheral blood of PCOS patients - a consequence of aberrant Il2 signaling. J Clin Endocrinol Metab. 2015;100(1):282–292. [PubMed: 25303485]
58. McLaughlin T, Liu LF, Lamendola C, et al. T-cell profile in adipose tissue is associated with insulin resistance and systemic inflammation in humans. Arterioscler Thromb Vasc Biol. 2014;34(12):2637–2643. [PubMed: 25341798]
59. Morris DL, Cho KW, Delproposto JL, et al. Adipose tissue macrophages function as antigen-presenting cells and regulate adipose tissue CD4+ T cells in mice. Diabetes. 2013;62(8):2762–2772. [PubMed: 23493569]
60. Wu H, Ghosh S, Perrard XD, et al. T-cell accumulation and regulated on activation, normal T cell expressed and secreted upregulation in adipose tissue in obesity. Circulation. 2007;115(8):1029–1038. [PubMed: 17296858]
61. Bertola A, Ciucci T, Rousseau D, et al. Identification of adipose tissue dendritic cells correlated with obesity-associated insulin-resistance and inducing Th17 responses in mice and patients. Diabetes. 2012;61(9):2238–2247. [PubMed: 22596049]
62. Viardot A, Heilbronn LK, Samocha-Bonet D, Mackay F, Campbell LV, Samaras K. Obesity is associated with activated and insulin resistant immune cells. Diabetes Metab Res Rev. 2012;28(5):447–454. [PubMed: 22492715]
63. Strissel KJ, DeFuria J, Shaul ME, Bennett G, Greenberg AS, Obin MS. T-cell recruitment and Th1 polarization in adipose tissue during diet-induced obesity in C57BL/6 mice. Obesity (Silver Spring). 2010;18(10):1918–1925. [PubMed: 20111012]
64. Sell H, Habich C, Eckel J. Adaptive immunity in obesity and insulin resistance. Nat Rev Endocrinol. 2012;8(12):709–716. [PubMed: 22847239]
65. Rausch ME, Weisberg S, Vardhana P, Tortoriello DV. Obesity in C57BL/6J mice is characterized by adipose tissue hypoxia and cytotoxic T-cell infiltration. Int J Obes (Lond). 2008;32(3):451–463. [PubMed: 17895881]
66. Nishimura S, Manabe I, Nagasaki M, et al. CD8+ effector T cells contribute to macrophage recruitment and adipose tissue inflammation in obesity. Nat Med. 2009;15(8):914–920. [PubMed: 19633658]
67. Liu S, Diao L, Huang C, Li Y, Zeng Y, Kwak-Kim JYH. The role of decidual immune cells on human pregnancy. J Reprod Immunol. 2017;124:44–53. [PubMed: 29055791]
68. Bishop CV, Xu F, Steinbach R, et al. Changes in immune cell distribution and their cytokine/chemokine production during regression of the rhesus macaque corpus luteum. Biol Reprod. 2017;96(6):1210–1220. [PubMed: 28575196]
69. Bishop CV, Xu F, Molskness TA, Stouffer RL, Hennebold JD. Dynamics of Immune Cell Types Within the Macaque Corpus Luteum During the Menstrual Cycle: Role of Progesterone. Biol Reprod. 2015;93(5):112. [PubMed: 26400401]
70. Yang X, Gilman-Sachs A, Kwak-Kim J. Ovarian and endometrial immunity during the ovarian cycle. J Reprod Immunol. 2019;133:7–14. [PubMed: 31055226]
71. Robertson SA, Moldenhauer LM, Green ES, Care AS, Hull ML. Immune determinants of endometrial receptivity: a biological perspective. Fertil Steril. 2022;117(6):1107–1120. [PubMed: 35618356]
72. Meza-Perez S, Randall TD. Immunological Functions of the Omentum. Trends Immunol. 2017;38(7):526–536. [PubMed: 28579319]
73. Benezech C, Luu NT, Walker JA, et al. Inflammation-induced formation of fat-associated lymphoid clusters. Nat Immunol. 2015;16(8):819–828. [PubMed: 26147686]
74. Tsai S, Clemente-Casares X, Zhou AC, et al. Insulin Receptor-Mediated Stimulation Boosts T Cell Immunity during Inflammation and Infection. Cell Metab. 2018;28(6):922–934 e924. [PubMed: 30174303]

75. Nojima I, Eikawa S, Tomonobu N, et al. Dysfunction of CD8 + PD-1 + T cells in type 2 diabetes caused by the impairment of metabolism-immune axis. Sci Rep. 2020;10(1):14928. [PubMed: 32913271]

76. Kavazovic I, Krapic M, Beumer-Chuwonpad A, et al. Hyperglycemia and Not Hyperinsulinemia Mediates Diabetes-Induced Memory CD8 T-Cell Dysfunction. Diabetes. 2022;71(4):706–721. [PubMed: 35044446]

77. Thomas AL, Alarcon PC, Divanovic S, Chougnet CA, Hildeman DA, Moreno-Fernandez ME. Implications of Inflammatory States on Dysfunctional Immune Responses in Aging and Obesity. Front Aging. 2021;2:732414. [PubMed: 35822048]

78. Porsche CE, Delproposto JB, Geletka L, O'Rourke R, Lumeng CN. Obesity results in adipose tissue T cell exhaustion. JCI Insight. 2021;6(8).

79. Cottam MA, Caslin HL, Winn NC, Hasty AH. Multiomics reveals persistence of obesity-associated immune cell phenotypes in adipose tissue during weight loss and weight regain in mice. Nat Commun. 2022;13(1):2950. [PubMed: 35618862]

80. Bradley D, Smith AJ, Blaszczak A, et al. Interferon gamma mediates the reduction of adipose tissue regulatory T cells in human obesity. Nat Commun. 2022;13(1):5606. [PubMed: 36153324]

81. Bishop CV, Takahashi DL, Luo F, et al. The combined impact of testosterone and Western-style diet on endometriosis severity and progression in rhesus macaquesdagger. Biol Reprod. 2023;108(1):72–80. [PubMed: 36173894]

82. Misumi I, Starmer J, Uchimura T, Beck MA, Magnuson T, Whitmire JK. Obesity Expands a Distinct Population of T Cells in Adipose Tissue and Increases Vulnerability to Infection. Cell Rep. 2019;27(2):514–524 e515. [PubMed: 30970254]

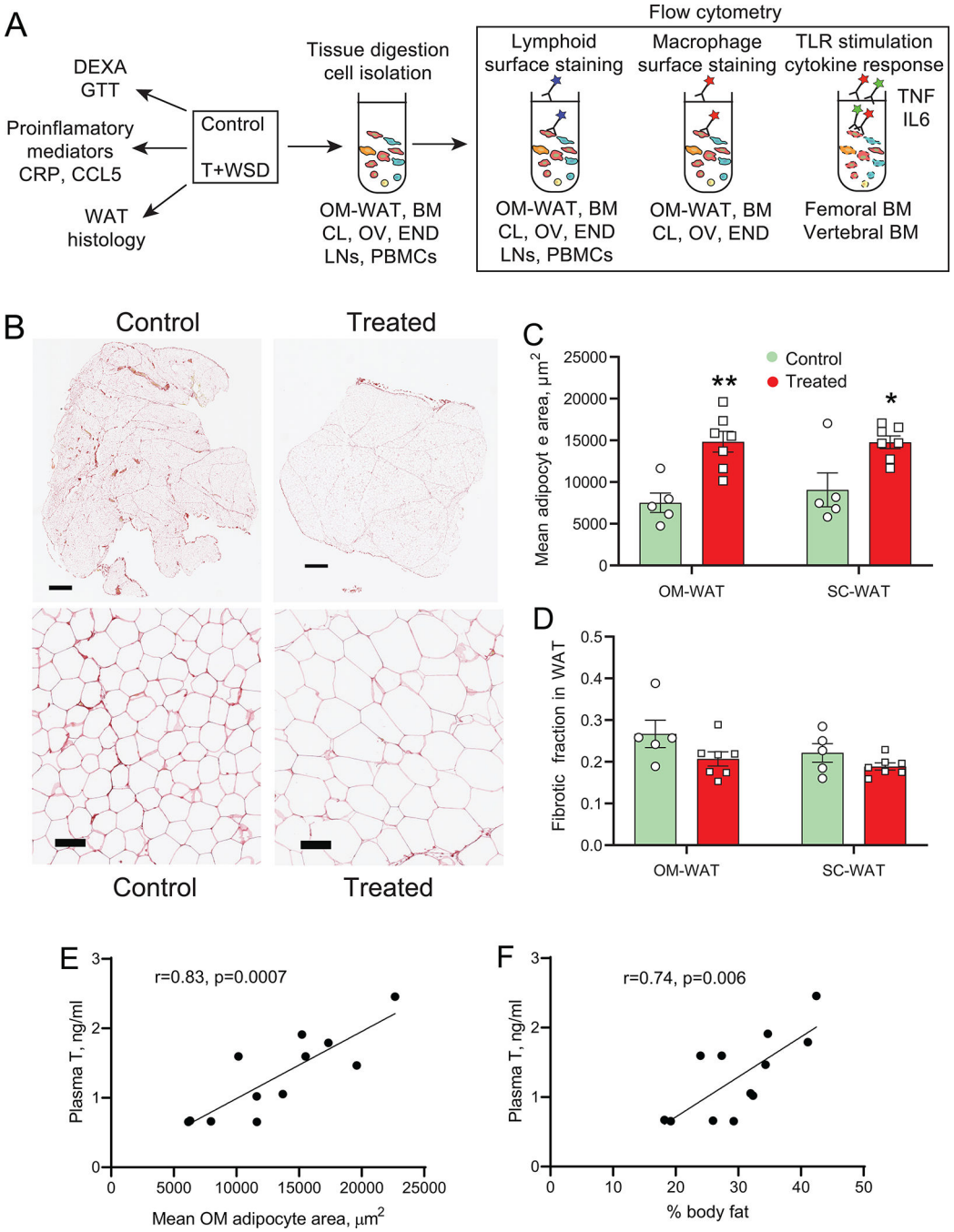

Figure 1. Effects of T+WSD treatment on adipocyte hypertrophy and WAT fibrosis.

(A) Experimental study design. Young adult female rhesus macaques were exposed to a low-fat control diet or an obesogenic Western-Style diet (WSD) in the presence of elevated circulating testosterone (T+WSD) for one year. Body composition and glucose tolerance were determined using DEXA and GTT. Circulating levels of C-reactive peptide (CRP) and Chemokine Ligand 5 (CCL5) were determined by ELISA. Adipose tissue was fixed, sectioned, and stained with picrosirius red. Immune cells residing in omental white adipose tissue (OM-WAT), corpus luteum (CL) and the contralateral ovary (OV),

endometrium (END), lymph nodes (LNs), bone marrow (BM), and peripheral blood mononuclear cells (PBMCs) were isolated and characterized by flow cytometry using lymphoid- and macrophage-specific antibody panels. Functional TNFα and IL6 responses of BM macrophages to Toll-Like Receptor (TLR) agonists were measured in femoral and vertebral (T12) BM. (B) Representative histological cross-sections of OM-WAT stained with picrosirius red; upper panels, whole-WAT scans used for the analysis (scale bars= 1 mm); lower panels, representative magnified regions of WAT (scale bars=50 μm). (C) Mean adipocyte size represented by the cross-sectional areas of OM and SC adipocytes of control and T+WSD animals. Each value represents the average adipocyte size per animal (1–2 whole-WAT scans were analyzed, see Supplementary Table 1 for details); 2-Way ANOVA, *$p<0.05$; **$p<0.01$. (D) Median fibrotic thickness in OM-WAT and SC-WAT of control and T+WSD animals. (E and F) Correlation between plasma testosterone (T) levels and mean OM adipocyte area (C) and a % body fat (n=12). Pearson coefficients and p-values are indicated.

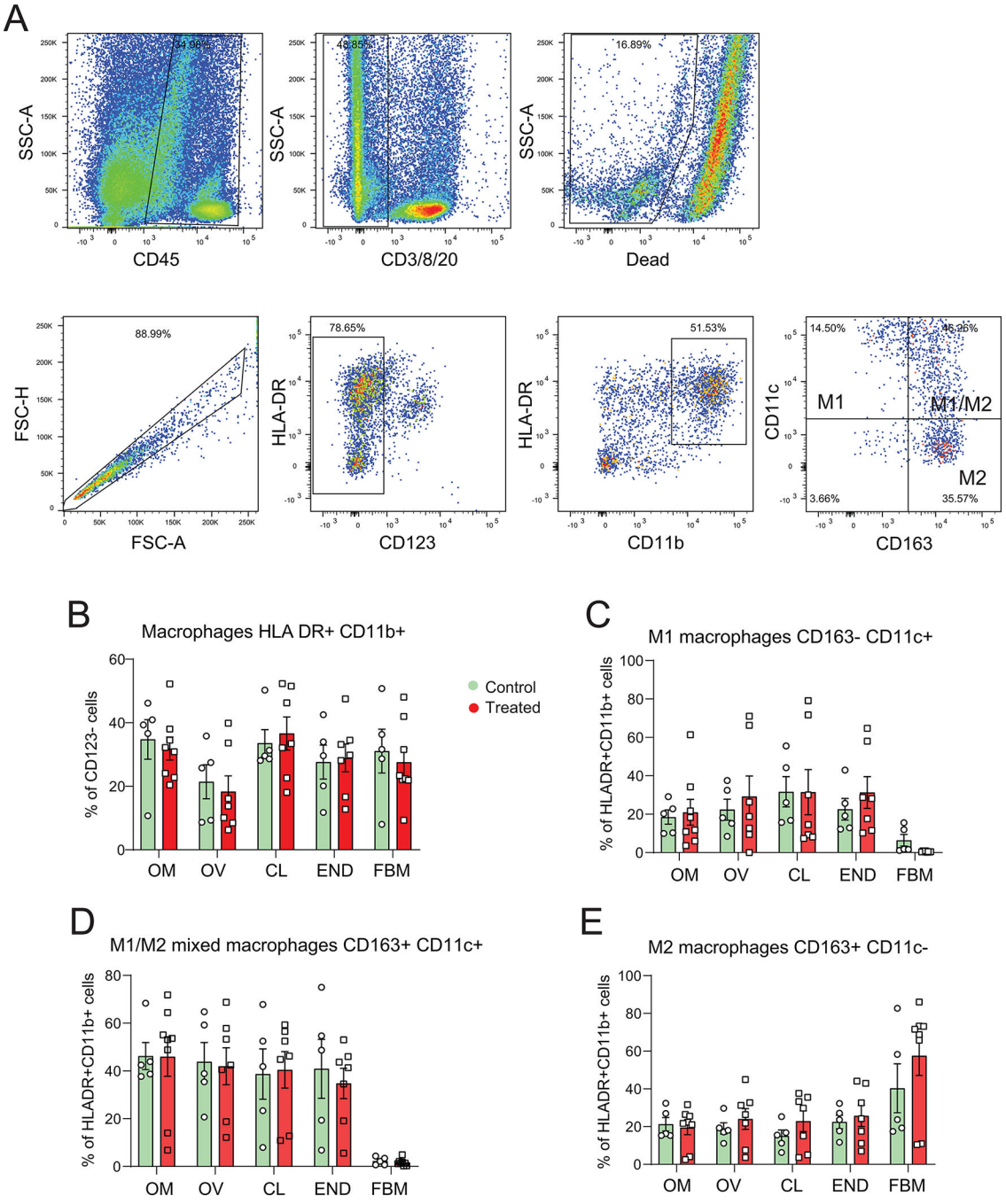

Figure 2. Effects of T+WSD on macrophage polarization.

(A) Macrophage gating strategy (OM-WAT; left-to-right): CD45+ immune cells->lineage-negative cells->live cells->singlets->CD123-negative non-dendritic cells->HLADR+CD11b+ macrophages->macrophage subpopulations are indicated. (B-E) Major macrophage subsets present in OM-WAT (OM), the corpus luteum (CL), the contralateral ovary not containing the CL (OV), endometrium (ENDO), the inguinal lymph node (ILN), and the femoral bone marrow (FBM). Bars are means ± SEM.

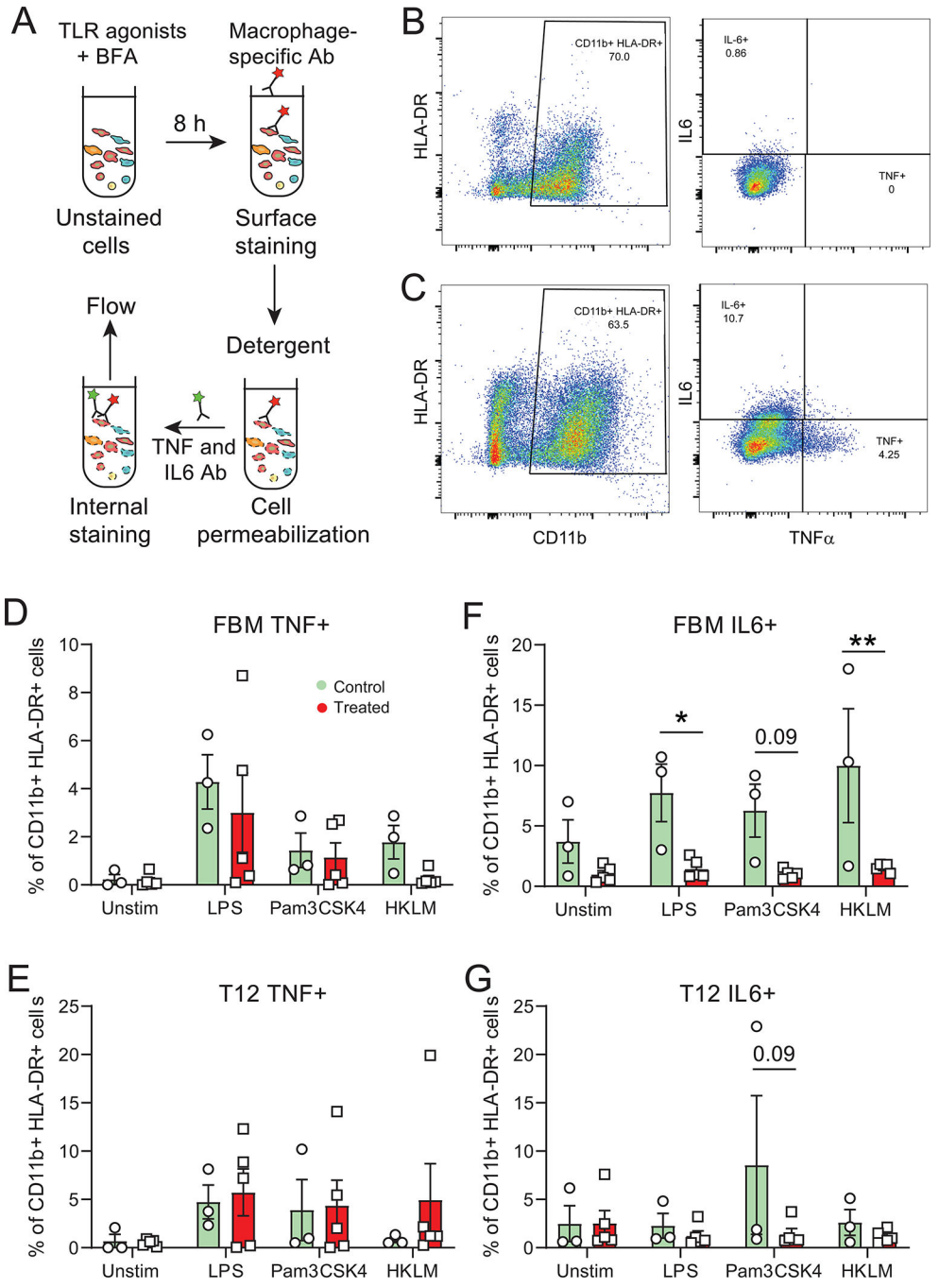

Figure 3. Effects of T+WSD treatment on macrophage function.

(A and B) Experimental design of macrophage function analysis and gating strategy. BM cells were incubated with control media, LPS (TLR4 agonist), Pam3CSK4 (TLR1/2 agonist), or HKLM (TLR2 agonist) in the presence of brefeldin A to enhance intracellular cytokine staining. Cells were stained with antibodies to CD11b and HLA-DR to delineate monocytes/macrophages. Following surface staining, cells were permeabilized and stained with monoclonal antibodies to TNFα and IL6 and analyzed by flow cytometry. (D-G) Frequencies of TNF+ (D and E) and IL6+ (F and G) macrophages in FBM (D and F) and

vertebral T12 BM (E and G) following stimulation with indicated TLR agonists; “Unstim,” unstimulated control. Bars are means ± SEM, 2-way ANOVA, *p<0.05, ** p<0.01.

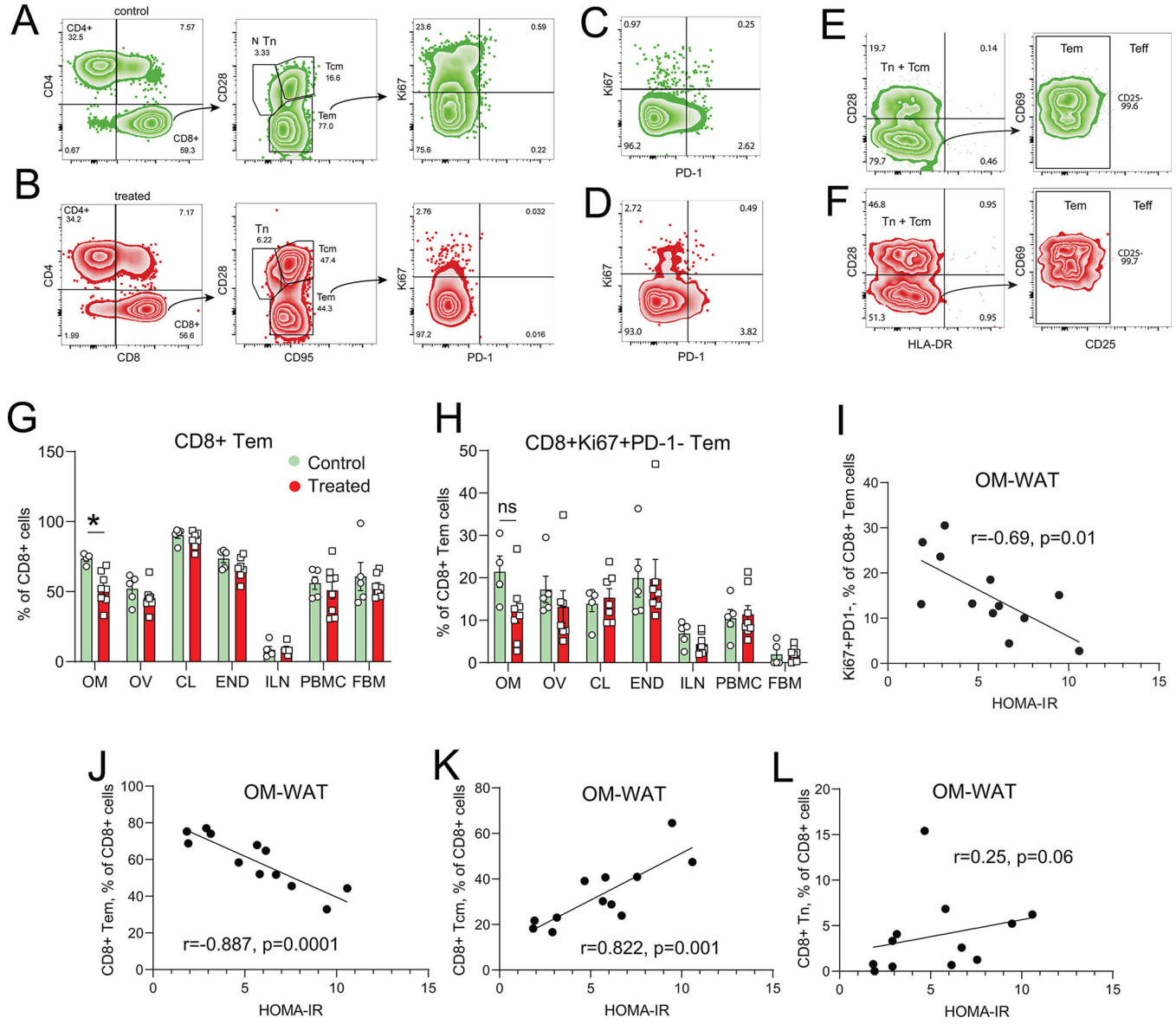

Figure 4. Effect of T+WSD on lymphoid phenotype.

(A and B) Gating strategy for analysis of CD8+ naïve (Tn), central memory (Tcm), and effector memory (Tem) cells from control (A) and T+WSD (B) animals (representative examples of OM-WAT analysis are shown). CD28- cells were sub-gated to delineate proliferating (Ki67+) and non-proliferating (Ki67-) T-cells expressing the PD-1 cell exhaustion marker. (C-D) Examples of PD1+ staining in the vertebral bone marrow of the control (C) and T+WSD (D) animals. (E-F) CD8+ cells were sub-gated to delineate populations containing non-activated HLADR-CD28- Tem and effector cells (Teff). (G) CD8+ Tn/Tcm frequencies in OM-WAT (OM), the corpus luteum (CL), the contralateral ovary not containing the CL (OV), endometrium (ENDO), the inguinal lymph node (ILN), and the femoral bone marrow (FBM). Bars are means ± SEM, 2-way ANOVA, *p<0.05. (H) Frequencies of proliferating PD-1-negative CD8+ Tem in various tissues (gating is shown in panel A); ns, not significant. (I-L) Correlation between frequencies of proliferating Ki67+

Tem (I), total Tem (J), total Tcm (K), and total Tn (L) and Homeostatic Model Assessment for Insulin Resistance, HOMA-IR. Pearson coefficients and p-values are indicated.

Table 1.

Effects of T+WSD treatment on metabolic and hormonal characteristics.

Parameters indicated were assessed in control and T+WSD groups at the time of necropsy; unpaired two-tailed t-test, p-values are indicated. HOMA-IR, Homeostatic Model Assessment for Insulin Resistance; AUC, area under curve.

	Control	SEM	Treated	SEM	T-test
Weight, kg	7.4	0.8	8.4	0.5	0.2064
Body fat, %	20.8	3.5	32.1	2.4	0.0057
Fasting glucose, mg/dL	54.6	0.6	62.8	2.4	0.0084
Fasting insulin, mg/dL	21.7	6.3	39.3	6.0	0.0393
AUC glucose	7128.1	556.5	9956.3	473.9	0.0007
AUC insulin	14168.3	5836.8	15163.9	2027.0	0.8158
HOMA-IR	2.9	0.9	6.2	1.0	0.0214
Testosterone, ng/mL	0.66	0.01	1.61	0.17	0.0025
CRP, ng/mL	337.8	113.6	432.4	62.2	0.3460
CCL5, pg/mL	57135.4	5506.1	39967.1	9040.1	0.1210

Table 2.

Correlations between immune cell frequencies in OM-WAT and metabolic and hormonal parameters.

CD8+ Tem	Fast glucose	Fast insulin	Glucose AUC	Insulin AUC	HOMA-IR	Body fat	OM adipocyte area	Plasma Testosterone
				-				
Pearson r	−0.6672	−0.8506	−0.7452	−0.2143	0.8867	−0.5913	−0.5504	−0.5344
R squared	0.4452	0.7235	0.5553	0.0459	0.7863	0.3496	0.3030	0.2856
P-value	0.0178	0.0005	0.0054	0.5037	0.0001	0.0429	0.0637	0.0734
Significance	*	***	**	ns	***	*	ns	ns
CD4+ Tem								
				-				
Pearson r	−0.2979	−0.4292	−0.4792	0.0650	0.4596	−0.1834	−0.1688	0.0022
R squared	0.0888	0.1842	0.2296	0.0042	0.2113	0.0337	0.0285	0.0000
P-value	0.3469	0.1638	0.1150	0.8409	0.1328	0.5682	0.6000	0.9946
Significance	ns	ns	ns	ns	ns	ns	ns	ns
M1 macrophages								
Pearson r	0.2038	0.1885	0.2152	−0.0403	0.2151	0.1492	−0.0239	0.1688
R squared	0.0416	0.0356	0.0463	0.0016	0.0463	0.0223	0.0006	0.0285
P-value	0.5251	0.5573	0.5018	0.9011	0.5020	0.6435	0.9412	0.6001
Significance	ns	ns	ns	ns	ns	ns	ns	ns

Correlation between frequencies of CD8+ Tem, CD4+ Tem, and M1 macrophages and indicated parameters. Pearson coefficient (r), R squared and p-value are indicated.

* p<0.05

** p<0.01

*** p<0.001

AUC, area under curve. HOMA-IR, Homeostatic Model Assessment for Insulin Resistance.